Biomimetic Survival Hydrodynamics and Flow Sensing

Biomimetic Survival Hydrodynamics and Flow Sensing

Michael S. Triantafyllou,[1] Gabriel D. Weymouth,[2] and Jianmin Miao,[3]

[1]Department of Mechanical Engineering, Massachusetts Institute of Technology
[2]Southampton Marine and Maritime Institute, University of Southampton
[3]School of Mechanical and Aerospace Engineering, Nanyang Technological University

Annual Review of Fluid Mechanics 2014.
:1–24

Keywords

Biomimetics, Maneuvering, Flow Control, Sensors, Robotics

Abstract

The fluid mechanics employed by aquatic animals in their escape or attack maneuvers, what we call survival hydrodynamics, are fascinating because the recorded performance in animals is truly impressive. Such performance forces us to pose some basic questions on the underlying flow mechanisms that are not in use yet in engineered vehicles. A closely related issue is the ability of animals to sense the flow velocity and pressure field around them in order to detect and discriminate threats in environments where vision or other sensing is of limited or no use. We review work on animal flow sensing and actuation as a source of inspiration, and in order to formulate a number of basic problems and investigate the flow mechanisms that enable animals develop their remarkable performance. We describe some intriguing mechanisms of actuation and sensing.

1. INTRODUCTION

The survival of marine animals depends on their capability to perform extremely rapid maneuvers, whether they escape predators, or attack prey in or out of the water, or jump upstream in water falls. Measured performance in live animals confirms the expectation that their function has been perfected through evolution. One can think of few instances when animal performance is more striking, as fish 30 cm long can reach accelerations exceeding ten times gravity acceleration in a fraction of a second and small squids can reach burst speeds of 25 body lengths per second. Such performance is based on underlying flow mechanisms, which are not currently used in engineered vehicles. Another critical element for survival is the ability of animals to sense the velocity and pressure fields around them in order to detect and discriminate threats in environments where other sensing is of limited use.

The intrinsic unsteadiness in the actuation of the locomotion of fishes becomes a major asset when large forces and moments must be generated rapidly in their escape maneuvers, reinforced by the flexibility and compliance of the body, fins, and wings of the animals. The interplay between vorticity generation and imparting momentum and hence kinetic energy to the fluid in order to power the animals survival hydrodynamics, is truly fascinating, as evolution has perfected animal function. In addition to rapidly maneuvering fish, we consider the cephalopods, such as the octopus and the squid, which are a particularly intriguing class of animals, because they incur large deformations and volume changes, forming shapes that apparently violate engineering rules of streamlining, yet achieving escape speeds matching those of the fastest animals, despite their lack of a skeleton. The cephalopods will serve as a prime example of bodies that undergo rapid shape changes, so that boundary layer vorticity can be shed simultaneously from large sections of their surface, in what is termed global vorticity shedding – and which allows them to develop their remarkable performance.

The ability of marine animals to detect their environment through pressure and velocity sensing is best exemplified by the blind cavefish that darts through cluttered cave environments in absolute darkness; and the harbor seal that detects the minute fluctuations in the wake of prey up to 30 seconds after it has passed. Survival has dictated the development of such hydrodynamic sensing that is totally absent from engineered structures. Again, we review work that poses some basic questions: How detectable is a flow from a localized distributed array of sensors? How can we detect flows down to 1 mm/s while moving at high speed?

Overall, we selectively review work on animal flow sensing and actuation in order to investigate those unsteady flow mechanisms that are employed by animals to develop their remarkable performance.

2. ESCAPE HYDRODYNAMICS

When fish or cephalopods attack or escape, they employ very large body and shape deformations, making the related flow-structure interaction problem radically different from that of rapidly maneuvering rigid hull vehicles. The measured performance in marine animals in terms of achieving high acceleration very rapidly is impressive, particularly because it is performed within a heavy liquid. The mechanics to develop the needed thrust require the rapid motion by the animal of a large mass of its surrounding water without incurring large drag and unrecoverable added mass forces; this simple remark will help us derive unifying principles of actuation.

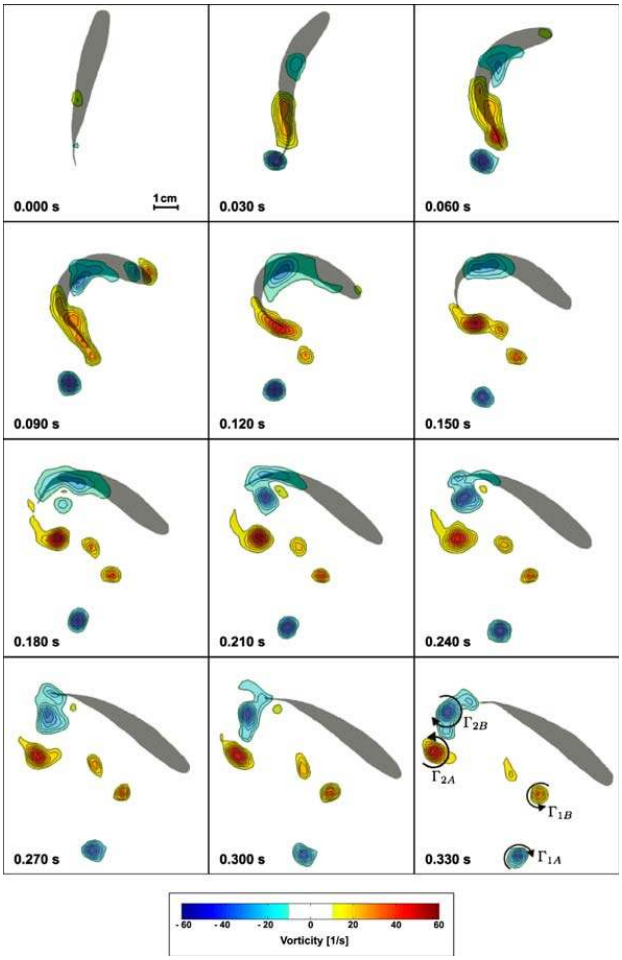

Figure 1: Sequence of vorticity field snapshots obtained through PIV at the mid-height planar cuts in the C-start of a danio fish; times as marked. Vortices marked Γ_{1A} and Γ_{1B} are cuts of the first vortex ring and Γ_{2A} and Γ_{2B} of the second vortex ring ((Epps & Techet 2007)).

2.1. Rapid Maneuvering through Large Body Flexing

Fast-starting fish employ large curvature flexing of their body to achieve impressive acceleration. In a series of articles reviewed in Domenici (2011), Webb explored the fascinating fast-starting performance of the trout, establishing the kinematics that lead to such accelerations: A first *preparatory* phase where the fish rapidly bends its body into a highly curved shape resembling either a letter C (*C fast start*), or a letter S (*S fast start*), followed by a second *propulsive phase* where the body is straightened out gradually, in a traveling wave-like fashion, starting with the head and ending with the tail (Webb (1976)), ultimately returning to its regular swimming mode. Work by Harper & Blake (1991) and Domenici & Blake (1997) provided data for other species, especially the pike, an aggressive fish whose

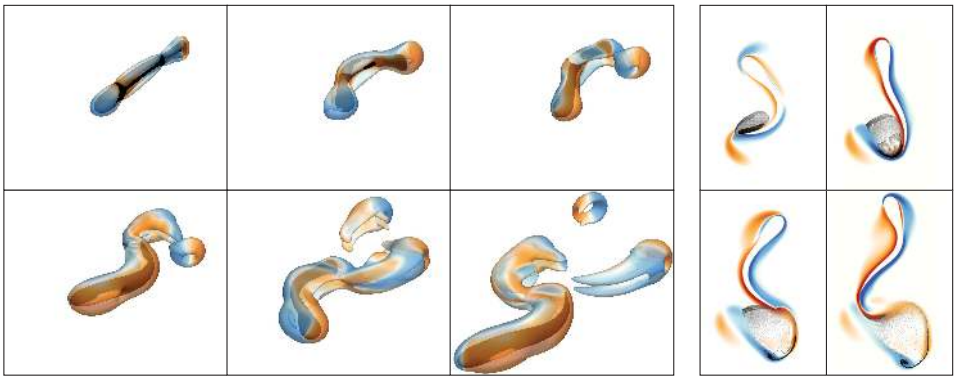

Figure 2: (Left) Vorticity field (z component of ω) in six snapshots (t/T_p= 0.13, 0.43, 0.71, 1.04, 1.61, 2.15, left to right, top to bottom) of the C-start maneuver of a larval fish, showing the formation of the actuating vortex rings. (Right) Evolution of passive tracer particles seeded at t/T_p= 0.5. Three sets of particles calored dark-medium-light grey are initialized at different regions and are overlaid on vorticity field (from Gazzola, Van Rees & Koumoutsakos (2012)).

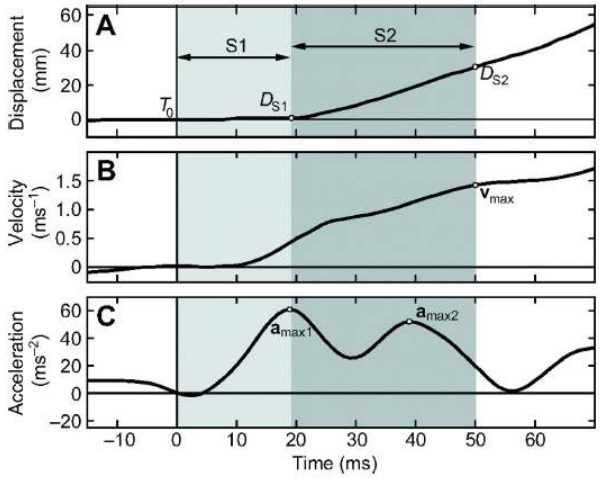

Figure 3: Displacement (upper), velocity (middle), and acceleration (bottom) as function of time in the two phases (S1, preparatory; S2 propulsive) of a C-start of a blugill sunfish that employs also its fins ((Chadwell et al. 2012)).

maximum acceleration is even more impressive than the trout's, exceeding ten times gravity acceleration. Fish that turn very rapidly while moving forward, employ maneuvers that resemble fast starts in many aspects, except that the initial phase, employed by a fish at rest to commence motion is not needed (Epps & Techet 2007; Wu, Yang & Zeng 2007).

Simple dynamic considerations show that a fast-starting fish must accelerate rapidly as large a mass of water as possible and move it in the proper direction: For a given

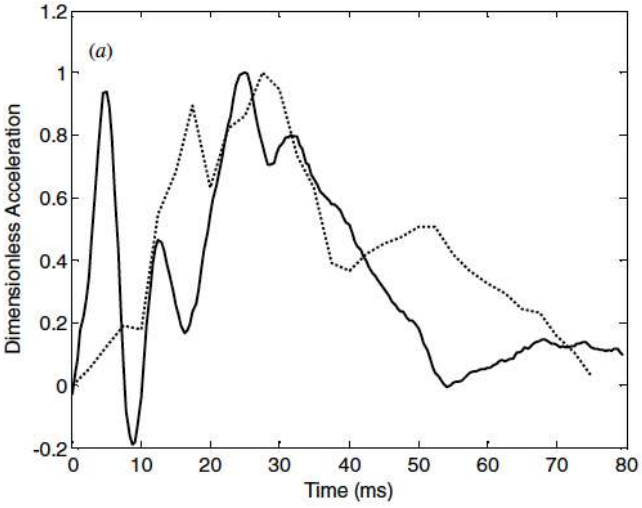

Figure 4: Experimentally measured acceleration in a fast-starting robot (solid line) versus acceleration measured in live fish (dotted line (Harper & Blake 1991)). Accelerations have been non-dimensionalized by their maximum values (from Conte et al. (2010)).

required fluid impulse, i.e. a given product of fluid mass and velocity, the energy that will be conveyed to the fluid is proportional to the product of mass and velocity squared, and, hence, is advantageous to involve a larger fluid mass so as to reduce the imparted velocity. The acceleration of fluid implies also the generation of vorticity, to be conveyed to the fluid as required by the kinematics of the accelerated flow; this vorticity must be generated at the body and fins of the fish, requiring a carefully choreographed motion driven by its muscles and fins working at full capacity and in a precisely timed manner. Hence, the available muscular power defines the limits of performance (Wakeling & Johnston 1998), but the use of suitable hydrodynamic mechanisms is critical to allow this escape to materialize. Figure 1 (Epps & Techet 2007) provides a sequence of PIV images of the vorticity in the flow around a turning danio. Initially, vorticity is confined to the boundary layer; as the fish moves, the vorticity entrains the kinetic energy imparted to the fluid through its large body flexing to form two vortex rings, a smaller one that powers the initiation of the turn and the rotation of the body, and then a stronger ring that provides the required force needed for the rapid acceleration. Borazjani et al. (2012) studied computationally a much faster C-start obtaining qualitatively similar results, but identified further vortical structures.

When reviewing the literature on live fish we must account for several complicating factors, because an escape maneuver involves first a stimulus from a predator, and is part of a predator-prey interaction problem (Weihs & Webb 1984). Hence, depending on the specific circumstances, the specific body shape employed (C-shaped versus S-shaped) provides different kinematics, while the use of fins can also vary, affecting the performance (Weihs 1973; Tytell & Lauder 2008). However, some basic fluid mechanisms emerge irrespective of

the specifics of actuation.

First, it is important to raise the question whether hydrodynamic considerations are the dominant factor in fast starts. To test this hypothesis, Gazzola, Van Rees & Koumoutsakos (2012) optimized through simulation a single type of maneuver (C-shaped), of a simply shaped fish (zebrafish larvae) that involves only its body and caudal fin. The criterion was to maximize the motion of the fish's center of mass within a given fixed time for both the preparatory and propulsive phases. Since the time is fixed, this criterion is also equivalent to maximizing speed or acceleration. The optimized kinematics closely resembled the observed live fish kinematics in Müller, van den Boogaart & van Leeuwen (2008), hence confirming the hypothesis that hydrodynamics dominate the kinematics of C-start.

Simulation allowed shedding further light on the actuation mechanics. Tracer particles were used to connect the flow features observed during the first phase of the maneuver, when the flow is largely irrotational, except within the boundary layer of the fish; with the vortical flow features obtained in the wake of the fish at the latter half of the maneuver. The vorticity shed in the wake flow is traced back to the surface of the body and caudal fin; more importantly, it is established that the mass of fluid, which is accelerated and "captured" by the body of the fish in the preparatory phase of the C maneuver, is either contained in or surrounds the vortical patterns of the wake flow, as shown in Figure 2. The irrotational-like flow at the preparatory phase, consisting of dipole-like structures at any particular planar cut that is perpendicular to the mid-line curve (as shown in Zhu et al. (2002)), transitions eventually to form two vortex rings. Hence, a principal conclusion of Gazzola, Van Rees & Koumoutsakos (2012) is that the strikingly large initial as possible: The body motion conveys significant kinetic (added-mass related) energy, which is then shed in the fluid together with body generated vorticity, to form two vortex rings powering the C-start. Hence, the initial potential flow-like added mass energy is used ultimately as propellant in this C-start maneuver (Triantafyllou 2012), a mechanism that is also employed under different conditions by cephalopod fast-starts, as shown in the next section.

Animals may employ their fins in an effor to better control the C-start but also increase the kinetic energy imparted to the flow during body bending. Figure 3 provides the kinematics of a blugill sunfish that employs its fins during a fast start. The two phases, preparatory and propulsive, are shown to produce peaks in the acceleration curve, which remains positive throughout the maneuver ((Chadwell et al. 2012)). In the study by Conte et al. (2010) a robotic device in the shape of a pike was tested by starting from a highly curved, C-like configuration, storing sufficient potential energy to drive a fast escape when released. By ommiting the preparatory phase, when significant added mass energy is imparted to the fluid that can be used as propellant, the acceleration fluctuates initially, to reach negative values, as shown in Figure 4, unlike the acceleration of a fast-starting fish. Still, the robot achieved a peak acceleration of 40 m/s^2 converting 10% of its initial energy to final kinetic energy, while the resulting kinematics are similar to those of fish.

2.2. Fast-Starts through Volume Change

Another group of animals to undergo large-scale deformations during escape maneuvers are the cephalopods: the octopus, cuttle fish, and squid. The octopus first hyper-inflates its mantle cavity filling it with water, which it then rapidly expels in the form of a propelling jet through the mantle orifice (Huffard 2006; Wells 1990; Packard 1969). As in the fast-starts of fish discussed above, there is a major advantage to accelerating as large a mass

of fluid as possible, hence the body inflation at the onset of the maneuver must be correspondingly large, increasing the lateral dimensions substantially. The normally streamlined mantle becomes quite bluff; flow around a similarly shaped rigid body geometry would incur large energy penalties in the form of flow separation drag and increased added mass force. However, the flexible, rapidly deflating mantle completely alters the dynamics of the flow, inducing mechanisms of separation elimination and added mass energy recovery, as investigated in Weymouth & Triantafyllou (2013), and demonstrated experimentally in Weymouth, Subramaniam & Triantafyllou (2015).

The core issue in determining the propulsive performance of the shrinking body is the evolution of the boundary layer vorticity at the external surface of the body as it undergoes large deformations. If this vorticity is shed into the flow, a drag wake will be established surrounding the propulsive jet emanating from the orifice, hence severely reducing the escape speed of the animal.

We first turn to the example of a shape change leading to vortex formation in G.I. Taylor's classic study (Taylor (1953)) of a vanishing disk. The solid disk is assumed to melt into fluid and the bound vorticity is assumed to roll up into a single vortex ring. Weymouth & Triantafyllou (2012) used viscous simulations to demonstrate that this assumption is mostly borne out in the case of a melting cylinder, whose diameter is reduced by 20%, and the resulting pair of vortices induces large drag forces. The study also found that the flow can be completely different depending on the form of the prescribed surface kinematics: If the body, instead of melting, collapses rapidly undergoing a prescribed shape change, as is more relevant to the octopus, then the vortex layer does not shed and roll up. Instead, it remains close to the body, while its total circulation decreases, as the body shrinks, through vorticity annihilation, as shown in Figure 5. As a result, instead of a purely resistive added-mass force and separation drag, rapid shrinking causes an additional added-mass related term in the form of positive thrust, through added-mass kinetic energy recovery, and near-elimination of viscous drag.

Both the circulation reduction and thrust force are due to the pressure gradient on the body, generated by rapidly reducing its volume. Consider the pressure distribution on the surface of a sphere of instantaneous radius R, translating at speed U in a potential flow:

$$p|_{r=R} = \frac{3}{2}\rho\left(\dot{R}U + \dot{U}R\right)\cos\theta + \frac{9}{16}\rho U^2\cos 2\theta + C(t) \tag{1}$$

where $C(t)$ is a constant over the surface and does not contribute to the force or generation of vorticity (Weymouth, Subramaniam & Triantafyllou 2015). For a rapidly shrinking body the first term implies very low pressure at the front of the sphere ($\theta = 0$) and very high pressure at the back ($\theta = \pi$). The two-dimensional form of this estimate was shown to be remarkably close to the viscous simulations of Weymouth & Triantafyllou (2012). This gradient generates a new sheet of vorticity on the surface of the sphere that lies directly under and has opposite sign than the boundary layer vorticity formed previously during the onset of translation. The induced normal velocity, pointing toward the surface, forces these two layers against each other, partially annihilating the boundary layer circulation. Recent experiments on flat plates recorded circulation reduction when rapidly changing the apparent cross-stream width of the body (Kriegseis, Kinzel & Rival 2013), which may arise from the same mechanism.

The pressure gradient also induces a thrust force on the body that transfers energy between fluid and body, of the form

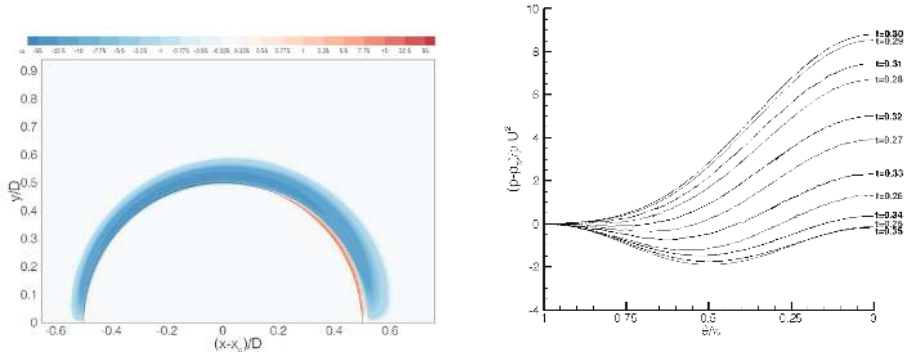

Figure 5: Left: Vorticity field from viscous simulations of a circular cylinder whose diameter shrinks rapidly by 20% as it moves from right to left. Right: The plot of the pressure on the cylinder surface (leading edge at left, trailing edge at right) at several snapshots marked by time, shows large, thrust-producing pressure gradient. The pressure gradient generates a sheet of opposite-sign vorticity (red color in back face of cylinder, left plot) under the previously formed boundary layer (blue color), resulting in vorticity annihilation. The pressure gradient generates thrust an order of magnitude larger than the steady drag on a rigid body (Weymouth & Triantafyllou 2012).

$$F_a = -\frac{d}{dt}(m_a U) = -\dot{m}_a U - m_a \dot{U}$$

where m_a is the instantaneous added-mass of the object. Solid bodies accelerating in a fluid experience an opposing force $-m_a\dot{U}$, but a shrinking body recovers fluid energy to develop thrust equal to $-\dot{m}_a U$, a term that dominates the overall force at the end of the maneuver. A consequence is that larger initial added-mass inertia is actually beneficial in the case of fast starts, as long as that inertia is recovered and released during the maneuver. The added-mass is fixed for a rigid vessel, making it, effectively, into an additional payload to be dragged along during the escape. In contrast, when the added mass energy is recovered and released, as fish do by bending and cephalopods do by shrinking, the body, effectively, turns their original added-mass into propellant. Spagnolie & Shelley (2009) also show this when a moving sphere undergoes a shape change to become a prolate ellipsoid, resulting in a sudden increase, or burst of velocity, as added mass momentum turns into body momentum. Quoting Spagnolie & Shelley (2009), "while a reduced virtual (added) mass gives a reduced acceleration reaction, a *reducing* virtual mass can generate a boost in velocity." For a self-propelled deflating body, recovery of fluid kinetic energy in inviscid flow, can accelerate it to speeds 82% greater than a rigid rocket, and even 20% greater than an ideal rocket in vacuum (**?**).

As implied by the pressure equation, the relative strength of this effect and the successful control of the viscous boundary layer is dependent on a non-dimensional shape-change rate, to overcome the rate of diffusion and separation in the boundary layer. As shown in Weymouth, Subramaniam & Triantafyllou (2015), it is insightful to compare a shrinking deformable body to the application of suction on a rigid body boundary layer, as both processes induce a normal velocity to the body surface, although shrinking induces it without

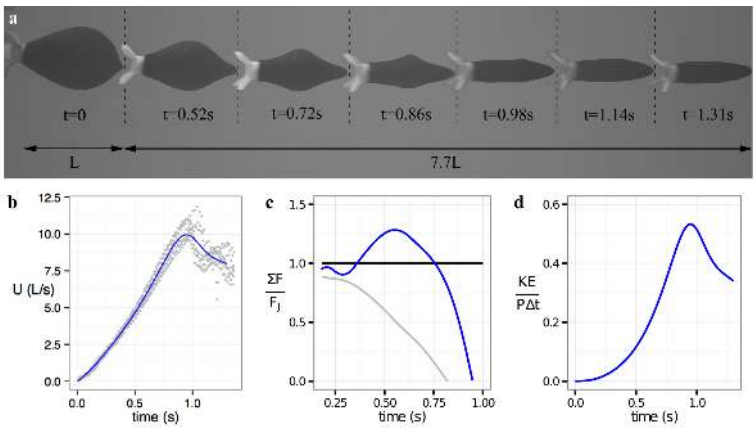

Figure 6: Self-propelled tests of an octopus-inspired rocket which propels itself via rapid large-scale shape change. A synthetic rubber membrane is stretched over a 3D printed rigid hull to power a fast-start maneuver which consistently achieves velocities greater than $10L/s$ in 1 s. 30% of the thrust is supplied by added-mass energy recovery, leading to efficiencies of more than 50% (Weymouth, Subramaniam & Triantafyllou 2015).

actual mass-flow through the membrane: A *deflation scaling parameter*, σ^*, was defined in analogy to the suction scaling parameter of a cylinder:

$$\sigma^* = \frac{\dot{V}}{AU}\sqrt{Re} \tag{2}$$

where $\dot{V}$ is the rate of change of the volume of the body, the Reynolds number is defined as $Re = UL/\nu$, and $A = \pi D^2/4$ is the frontal area. For a sphere, an estimated threshhold value of σ^* is 2.41π. Hence, the required deflation rate decreases with Reynolds number, which was confirmed by the viscous simulations and the experimental testing of a robot (Weymouth & Triantafyllou 2013; Weymouth, Subramaniam & Triantafyllou 2015). As shown in Figure 6, the robot experiences an instantaneous thrust force 30% greater than the thrust provided by the propulsive jet (and avoids a 50% reduction in the net force due to drag forces as in a rigid body), resulting in a fast-start maneuver with 53% hydrodynamic efficiency.

Other soft and deforming animals and mechanisms may employ similar mechanisms to help with their efficient periodic propulsion.

2.3. Unifying principles in fish and cephalopod fast-starts

Fish employing C-starts and cephalopods escaping through rapid deflation of their initially hyper-inflated mantle, are found to use the same principles: Fish engage into large curvature maneuvers to impart large kinetic (added mass) energy to the fluid, which is entrained and released in the vortex rings that power their maneuver. Similarly, escaping cephalopods are initially bluff, imparting large kinetic (added mass) energy to the fluid, which they recover as they deflate rapidly to produce thrust in the later stages of their maneuver, when it is most useful, because their mass is substantially less as they have expelled fluid from their mantle.

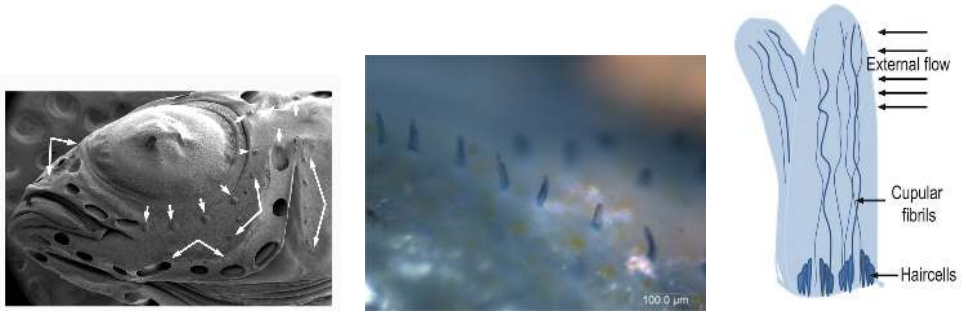

Figure 7: (Left) Electron micrograph of juvenile cichlid fish with body length $\approx 11\ mm$ shows lateral line canals with large pores; presumptive CN under eye that will be enclosed in canals when older (short arrows); and SN (double arrows); opening between arrow heads on snout is the nostril (Webb 2014b). (Center) Microscopic image of an array of cupulae of superficial neuromasts on the body of the fish, dyed with methylene blue (McConney et al. 2009b). (Right) Schematic of a surface neuromast and cupula subject to flow (Kottapalli et al. 2013).

However, this performance is conditional on avoiding unontrolled flow separation. In the case of the fish, a highly choreographed motion ensures that the fish does not create large angles of attack with respect to the flow. In the case of cephalopods, a more intricate mechanism of separation elimination is employed as deflation must be rapid enough to create opposite sign vorticity to partially eliminate the boundary layer vorticity and impose a normal velocity component to the body surface that prevents separation. Both components are equally important so that the fluid kinetic energy is recovered by the body rather than be shed to the fluid together with the excess boundary layer vorticity.

3. FLOW SENSING IN AQUATIC ANIMALS AND MARINE VEHICLES

For fish survival, timely and accurate sensing is as important as agile actuation, whether it is to avoid predators or detect prey. For example, C-starts can generate strong and long-lasting flow signatures (Niesterok & Hanke 2012), and swimming fish can be tracked via their wake long after they have passed. While vision, hearing, and smell are also employed, many aquatic animals possess the unique ability to detect prey or predator and even form a three-dimensional map of the surroundings by sensing the velocity and pressure fields through multiple sensors distributed along their body. We first review selectively the literature on the physiology (structure, size, location, and density of the sensors) and reported function of the animal sensors, in order to first assess the feasibility and limitations of sensing the flow, and then review the efforts to replicate this function with engineered sensors.

3.1. Flow sensing: The lateral line of fish

Detailed, excellent recent publications provide rich information on the function of animal sensing (Coombs et al. 2014; Bleckmann, Joachim & Coombs 2014). Fishes utilize cues from their lateral-line system, so named because its most visible part is a line of scales running down the side of the fish, to locate predator or prey and underwater objects, and

form schools (Chagnaud & Coombs 2014; Webb 2014b; Pitcher, Partridge & Wardle 1976). The capabilities of this organ are best exhibited by the blind cave fish, *Astyanax mexicanus fasciatus*, because of its lack of functional eyes. Cave fish, typically up to 10 cm in length, live in dark caves and have atrophied eyes, but are capable of forming a three-dimensional map of their surroundings by sensing flow velocity and pressure variations (Montgomery, Coombs & Baker 2001; Von Campenhausen, Riess & Weissert 1981).

The sensory units of the lateral line, the neuromasts, are spread across large portions of the surface of the fish body. Each neuromast sensor consists of haircells that are embedded into a cupula containing a soft gelatinous material. Each hair cell consists of a long kinocilium and an attached bundle of stereocilia, shorter and graded in height. The haircells are connected to the afferent fibers at the base and form the principal sensing element. There are two types, superficial neuromast (SN) sensors with haircells as shown in Figure 7, that are freestanding on the surface of the skin and exposed to the flow, and canal neuromasts (CN) that are embedded inside lateral-line canals (Coombs et al. 2014; Montgomery, Baker & Carton 1997; Abdel-Latif, Hassan & von Campenhausen 1990; Montgomery, Coombs & Baker 2001; Webb 2014a).

There are differences between SNs and CNs stemming from their distinct morphology, such as the difference in the shape of the cupula (CN has a hemi-spherical shape with hundreds of microns in diameter, while the SN cupula is oval-shaped, 10 to 60 microns wide and 50 to 400 microns high). Also, SN typically contains roughly 10, while CN contain hundreds, or even sometimes thousands of haircells (van Netten 2006). The cupula of an CN is found to "slide" on its epithelium like a rigid body resisted by spring-like hair bundles, unlike the elongated cupula of an SN, which bends in the flow like a beam. Both SNs and CNs contain two groups of oppositely oriented haircells that are spatially intermingled.

SNs have high sensitivity for flow sensing, and can even sense the flow created due to planktonic prey in water. At a frequency around 100 Hz displacement of 1 nm is sufficient to cause a neural response, while displacements greater than 100 nm cause saturation of individual hair cells (van Netten 2006).

CNs are embedded in subdermal canals and are exposed to the flow through pores (Figure 7), whose walls are formed by rigid structures, such as bone or scale. The canal lateral line system consists of a trunk canal and cephalic canals. The trunk canal typically consists of one or multiple linear canals which run laterally down each side of the body, while the cephalic canals are complex and form a 3-D pattern around the head (Webb 2014a). A single neuromast is embedded between two pore openings, actuated only when there is a pressure difference between the consecutive pores. The motion of water inside the canal is impeded by the inertia of water and the friction offered by the canal walls. At low frequencies, the friction generated by the walls of the canal is dominant (Montgomery, Coombs & Halstead 1995), while at high frequencies the mass of fluid in the canal acts as a low pass filter. As outlined in van Netten (2006), the mass of the CN cupula and the stiffness induced by the large number of haircells result in a resonance frequency below 100 Hz, whose ultimate effect is to render the sensor sensitivity flat up to a frequency of roughly 100 Hz. The CN acts effectively as a band pass filter of oscillatory pressure gradients.

The fact that neuromasts are concentrated at locations where changes in pressure are greatest during motion through water, while their morphology changes as fish develop through the embryonic, larval, and juvenile stages, points to the continuous optimization of the location of these sensors for best flow sensing (Ristroph, Liao & Zhang 2015; Webb

2014a).

The lateral dimension of SN is of the order of 100 microns so for flow speeds up to 1 m/s the Reynolds number is below 100 in open flow; hence accounting for the effect of the boundary layer thickness, which is typically larger than the SN height, the relevant Reynolds number is even smaller (McHenry & Liao 2014). As a result, the force on SN is largely viscous, while it is unlikely for the neuromast to develop a Kármán street, whose unsteady fluctuations would cause considerable measurement noise. Likewise, the internal flow in the canal due to external pressure gradients is likely to be far smaller than 1 m/s, arriving at similar conclusions for the CN, despite their larger size. It is estimated that, as a lower threshold, CN can respond to internal velocities down to 1 to 10 $\mu m/s$ or accelerations 0.1 to 1 mm/s^2; and SN to 25 to 60 $\mu m/s$ (van Netten 2006; Rapo et al. 2009).

3.2. Forming three-dimensional images through near-body flow sensing

The lateral line is known to help fish perform complex sensing tasks, such as detecting threats to spark C-starts, as well as assisting in Kármán gaiting through vortex detection (Liao 2006, 2007). The central question is on the possibility of forming a three-dimensional map of the flow, at least in the vicinity of the fish, through velocity and pressure measurements obtained using multiple sensors spread over a specific area of a moving body, such as the SN and CN of the lateral line of fish.

3.2.1. Flow reconstruction: Inviscid theory. For two-dimensional inviscid flow it can be shown that a body moving in prescribed motion around another body can use distributed measurements over some time to create a complete map of the flow, provided the two bodies are in relatively close proximity, of the order of one body length or less (Sichert, Bamler & van Hemmen 2009; Bouffanais, Weymouth & Yue 2010); the presence of an external flow makes identification easier. Bouffanais, Weymouth & Yue (2010) analyzed the mapping of the environment via pressure signals in two ways, first to determine the pressure signal of a given obstacle shape and then to find the location and shape of a body given its pressure signal. They found that insufficient information is provided about the shape by a pressure signal at a single location. The information regarding the size, orientation, and position decays proportionally to $1/d^2$, $1/d^2$, and $1/d^3$, respectively, where d is the distance between the sensor and the body. An unscented Kalman filter was used with noisy pressure signals, obtained as the sensor moves around an object, to detect the position and shape of the pressure-generating body. It was found that the fish has to be within a distance of $6D$, where D is the size of the object, to detect size; and within $3D$ to detect position. Obtaining any further details of the shape requires an even closer distance.

Windsor et al. (2010) studied the effects of a fish gliding parallel to a wall in close proximity, and found that detection is possible at distances less than 10% of the length of the fish.

Gao & Triantafyllou (2012) used pressure sensor arrays in a maneuvering underwater vehicle to detect flow direction using unscented Kalman filtering, and use it in a feedback loop to control its orientation. A critical element in the controller during vehicle linear or angular acceleration was to subtract the pressure caused by the vehicle's own motion (added mass-related pressure).

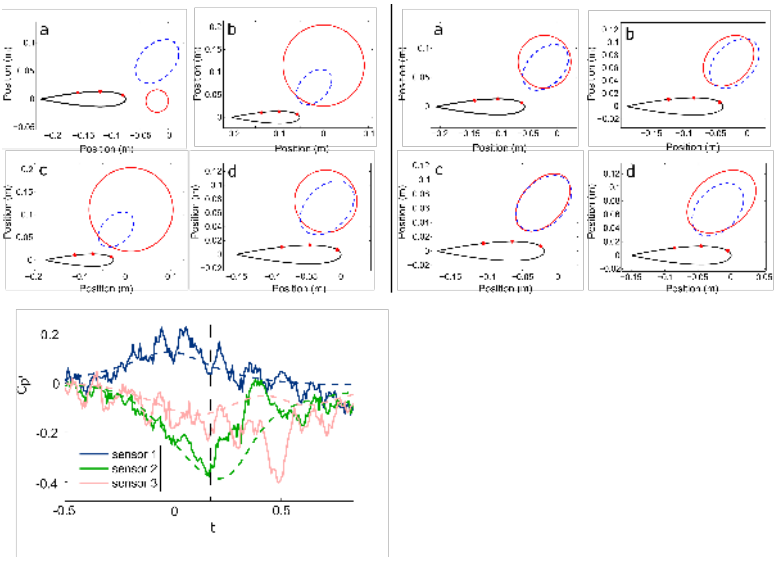

Figure 8: Upper figure: Snapshots of experimental shape identification of a an elliptical cylinder using three pressure sensors placed on a gliding foil of chord $c = 10$ cm (red dots on foil denote sensors: 1 is near the nose, followed by sensors 2 and 3); dotted blue line denots the true, and solid red line the estimated position and shape. Left figures a, b, c, d are results from a first pass; on the right are from a second pass that used the first pass results (Fernandez et al. 2011b). Lower figure: Pressure measurements from the three sensors as function of relative position between the foil leading edge and cylinder right edge, x/c; note large oscillations beyond $x/c = 0.20$, when the cylinder is above the middle of the foil (Maertens & Triantafyllou 2014).

3.2.2. Flow reconstruction: Viscous effects. In viscous flows, potential flow methods become invalid once flow separation occurs, while there are no direct methods for object identification. Fernandez et al. (2011b) used a streamlined body instrumented with an array of seven commercially available pressure sensors, to estimate the position and velocity of a bluff cylinder translating in close proximity, after first identifying the principal features of its vortical wake by performing a principal component analysis on a set of training data. A clear differentiation could be made between a circular cylinder and a square cylinder, for example.

Bleckmann & Zelick (1993) towed objects in linear or slightly curved paths very close (1 cm) to electric fish. Responses increased with object speed eventually showing saturation. As distance increased, the response decayed as a power function of distance. Müller, Fleck & Bleckmann (1996) towed a rectangular object on a circular orbit at various speeds near a catfish and Mogdans & Bleckmann (1998) close to a goldfish, eliciting responses that increase with the speed of towing. The peripheral lateral line units of the goldfish responded with predictable patterns. Plachta (2003) towed a sphere 8 mm in diameter at constant speed close to a goldfish, and found three types of response: Some lateral line units (likely to be SN) responded maximally when water velocities across the surface of the fish increased due to sphere movement; other units responded only while the sphere passed a certain location

on the fishs head or body, but did not positively correlate with the water motions at that location; and a third type that discharged only after the sphere had passed the fish.

Fish receive stimuli from external disturbances, but also from flow disturbances caused by their own motion. This requires two strategies, first to switch off sensor input in the absence of external stimuli, and second the capability to store the self-made flow noise patterns, so as to "subtract" them from the total sensory input (Von Campenhausen, Riess & Weissert 1981). As expected, an actively flapping fish generates more noise, hence fish have a sensory advantage when gliding.

Fish are known to wander about obstacles (Von Campenhausen, Riess & Weissert 1981). Fernandez et al. (2011a) employed potential flow methods and unscented Kalman filters to experimentally detect the position and shape of a cylinder or ellipse using noisy pressure measurements obtained over a period of time at three locations on a streamlined foil gliding at constant speed in close proximity. As shown in Figure 8, a first pass by the foil allowed a good first approximation of the location and size of the cylinder, and then a second pass allowed a very accurate estimate of both. However, once the foil went past the cylinder, strong vortical structures emanated from the foil due to hydrodynamic interaction with the cylinder, causing large pressure oscillations in the measurements (Figure 8).

For simple objects, pressure measurements up to the point when flow separates may be sufficient for detection, but generally this is a serious limitation for inviscid methods. Maertens & Triantafyllou (2014), however, showed that the dominant frequency and wavelength of these unsteady vortical structures develop as a result of an instability of the average shape of the boundary layer profile of the foil and, hence, can be predicted using instability theory. This instability amplifies the potential flow-like disturbance caused in the front part of the foil, and since the form of these disturbaces is specific to the cylinder shape that generated them, they were further used to identify its shape. The findings support the intriguing possibility that the significant unsteady viscous effects caused by nearby bodies on the fish boundary layer, far from preventing detection, could be used by animals to better identify objects.

3.2.3. Tracking swimming fish: The pulsating dipole analogy. At relatively small distances away from a vibrating, constant-volume, flexible body, the leading hydrodynamic term is that of an oscillating-strength dipole. Hence, the pulsating dipole flow generated by a harmonically vibrating rigid sphere has become the canonical model for studying the detection of swimming fish or zooplankton when their wakes are not involved. Mottled sculpin around 10 cm in length, for example, will strike at a vibrating sphere in the dark when placed within a distance roughly equal to their length (Coombs & Conley 1997).

Montgomery, Coombs & Baker (2001) have conducted experiments on live blind cave fish using a vibratory dipole stimulus to generate unsteady flow combined with a steady flow generated in a water tunnel. An anesthetized live fish is positioned in the test-section of the water tunnel and the electrical impulses from both the SNs and the CNs are recorded as function of the frequency. A constant flow velocity of the stimulus is obtained by progressively reducing the amplitude of vibration, as vibration frequency is increased.

Hassan (1993) showed that the flow, generated by a vibrating sphere near the cast model of a blind fish has characteristic patterns that can be detected by distributed SN, provided the (potentially strong) effects of the boundary layer are accounted for; and by distributed CN if the effect of the orientation of the canal relative to the position of the sphere has been accounted for. Curcic-Blake (2006) used a teflon sphere with 5 mm diameter vibrating in a

direction roughly parallel to a ruffe lateral line canal, 10 cm in length, at a frequency around 70 Hz, placed at distances of the order of 10 mm. The hydrodynamic signals detected by the lateral line have sharply characteristic shapes as function of length, allowing precise detection of the sphere's location, and amplitude and frequency of oscillation. There is a lower detection threshold, estimated at $2D_s$, where D_s is the distance between two adjacent pores, and an upper distance threshold estimated at $L/\sqrt{2}$, where L is the length of the lateral line canal. Consistent with the idea of detecting the pulsating sphere through its spatial signature, striking fish employ strategies that keep the sphere lateralized (Coombs & Conley 1997).

Rapo et al. (2009) studied the flow effects on a fish-like body due to an oscillating sphere. The unsteady boundary layer on the fish has typical thickness 80 μm at $80Hz$ and alters the magnitude and phase of the velocity within this distance. Potential flow can calculate relatively accurately the pressure gradient patterns to the lateral line system but not the velocity field, because of the oscillatory boundary layer on the skin of the fish.

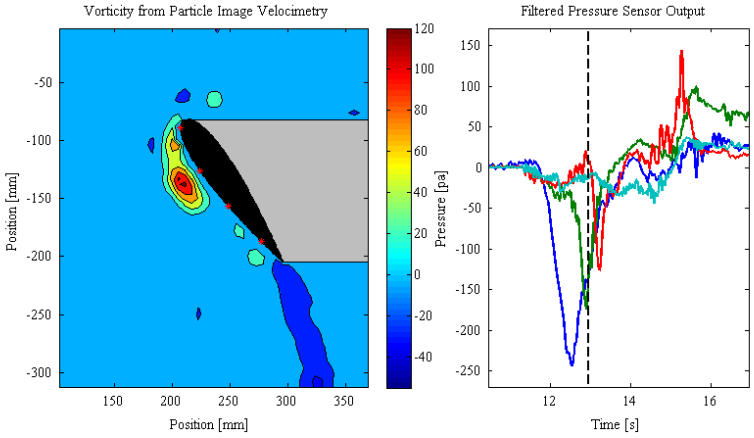

Figure 9: Vortex detection on a stalling foil at an angle of attack of 35 deg., translating at 0.3 m/s, equipped with four pressure sensors (red dots on foil). Left: vorticity field obtained via PIV; a shed LEV is clearly visible adjacent to the second sensor. Right: time trace of pressure at the sensors, starting from the leading edge: 1 (blue); 2 (green); 3 (red); 4 (green). Vertical dotted line is at time corresponding to the frame at left (Fernandez et al. (2011a)).

3.2.4. Tracking vortical structures with neuromasts. Fish generate strong vortices and form wakes for their propulsion and maneuvering, hence tracking other fish or forming schools requires the detection of vortical structures. The characteristic low pressure signature of a vortex makes it easily detectable through pressure sensing, hence it is anticipated that this is a function primarily for the CN, although SN arrays can also assist. Also, fish motion within vortical flows requires sensing of oncoming vortices. Trout placed behind a bluff cylinder are capable of extracting energy from the oncoming wake (Liao et al. 2003) by slaloming through the Kármán street vortices; hence they must have a sensing capability of vortices. Beal et al. (2006) showed that with pressure sensors it is possible to extract net energy from a Kármán street using a flapping foil. Liao (2006) studies the effect of vortical

flows on the lateral line of trout, finding that the lateral line plays a greater role than vision in holding station in a Kármán street.

Chagnaud, Bleckmann & Engelmann (2006) stimulated the lateral line of a goldfish with a vortex ring that passed the fish laterally from anterior to posterior at a close distance. They concluded that fish might be able to extract sensory information from complex stimuli like vortices by comparing the activity of a whole array of neuromasts

A number of authors have established the feasibility of tracking vortices and vortical wakes: Yang et al. (2006) for vortical wakes; Ren & Mohseni (2012) for regular or reverse Kármán vortex street using CN-like sensors distributed over the surface of a body, which provide sufficient information to extract the circulation of individual vortices, the wavelength of the Kármán street, the distance between the body and the fish h and the speed of propagation of the street. Likewise, Akanyeti et al. (2011); Venturelli et al. (2012); Salumae & Kruusmaa (2013), and Chambers et al. (2014) demonstrated using an array of pressure sensors that it is feasible to extract features from the flow such as the vortex shedding frequency, traveling speed, wake wavelength, and turbulence intensity.

Fernandez et al. (2011a) determined the strength and position of a free vortex pair translating near a streamlined body using sparse pressure sensor measurements and a potential flow model with an extended Kalman filter, comparing it to simultaneous PIV measurements. Also, an array of pressure sensors mounted inside a model sailboat hull was used to identify helical vortex shedding from the keel line. Finally, it was shown that the characteristic pressure signature of a vortex is detectable through the use of even a small number of sensors, as shown in Figure 9.

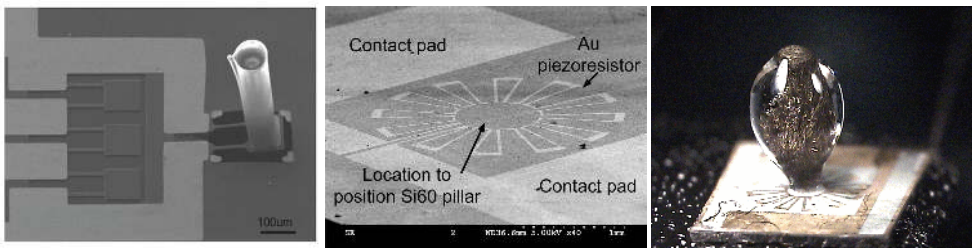

Figure 10: Biomimetic MEMS sensors. (Left) Sensors featuring SU-8 hair cells, 700 microns tall, located at the distal end of a micro-cantilever with embedded piezoresistors at the hinge demonstrated ultra-high sensitivity in sensing flow velocity and direction (Liu (2007)). (Center) Image of an LCP membrane (diameter 2 mm) pressure sensor (Kottapalli et al. (2012a)). (Right) Piezoresistive sensor with cupula and encapsulated nanofibers (Kottapalli et al. (2013)).

3.3. Biologically inspired and Biomimetic MEMS sensors

MEMS and NEMS (Micro/Nano-electro-mechanical systems) technology offers unique advantages for developing inexpensive, low-power arrays of micro-flow and pressure sensors emulating the function of the lateral line. Inspired by the neuromasts on various species, Yang et al. (2006, 2011); Chen et al. (2007); Dagamseh et al. (2012, 2013); Tao & Yu (2012); McConney et al. (2009a), and Klein & Bleckmann (2011) developed MEMS-based sensors using piezo-resisitive and piezo-electric materials, resistive polymer, capacitive as well as

optical methods to convert the flow-induced deflection of pillars, rods, bars or membranes to electrical signals.

Figure 10 shows an artificial SN-like velocity sensor (Liu 2007). Most research focused on developing single flow sensors based on the SN structure, while the CN structure has received less attention (Ren & Mohseni 2012). McConney et al. (2009b) and Kottapalli et al. (2013) developed biomimetic SN-like structures with an artificial cupula, proving that sensitivity can be enhanced by at least an order of magnitude.

Targeting real-time flow sensing on unmanned underwater vehicles, Kottapalli et al. (2011, 2012a,b, 2013); Coombs et al. (2014); Miao et al. (2013); Asadnia et al. (2013a,b); Fernandez et al. (2011b), and Dusek et al. (2013) adapted a bio-inspired approach, eliminating the fragile haircell element of the sensor and developed lateral-line inspired flexible arrays of polymer MEMS sensors, and self-powered piezoelectric sensors. Polymer sensors were developed using liquid crystal polymer (LCP) as a sensing membrane material, because it is far more robust for underwater applications than silicon (Kottapalli et al. 2011; Miao et al. 2013; Kottapalli et al. 2011, 2012a,b). The haircells (less than 1 mm in height) did not extend beyond the boundary layer generated by the flow (Chen et al. 2007; Dagamseh et al. 2012, 2013). Kottapalli et al. (2012a) reported a biomimetic SN polymer MEMS flow sensor using an LCP membrane, a high-aspect ratio and 3-mm high Si60 polymer haircell, fabricated stereolithographically, as shown in Figure 10. Through proper material selection and design, the sensitivity of the device is enhanced without compromising the robustness.

CN-inspired sensors placed in a canal were developed by Kottapalli et al. (2014a) The distance between two artificial canal pores is 6 mm and the canal pore diameter 1 mm. Klein & Bleckmann (2011) developed artificial lateral-line canal sensors that use optical sensing by determining the flow-mediated light transfer efficiency through tiny silicon bars (that act as hair cells) embedded into canals.

Dusek et al. (2013) conducted field experiments using an autonomous surface vehicle equipped with three experimental pressure sensor arrays complemented by commercially available sensors. Two flexible arrays were developed using a silicon piezoresistive sensor die mounted on liquid crystal polymer, and flexible PCB substrates, respectively. The third sensor array was developed using carbon black PDMS (CBPDMS) composite patterned in a strain gauge arrangement on a flexible PDMS substrate. It was demonstrated that the vehicle steady and transient motions could be detected accurately based on the pressure measurements of all three sensor designs.

3.4. Tracking wakes with pinniped whiskers

Observations on pinnipeds, such as sea lions and harbor seals, revealed an impressive ability for prey tracking. Dehnhardt, Mauck & Bleckmann (1998) studied the response of a harbor seal to dipole stimuli showing their ability to detect minute water movements, as low as 0.3 mm/s. Subsequent studies Dehnhardt (2001) showed that a blindfolded seal is capable of following the trail of a small model submarine, even after 30 s had elapsed, when the wake defect velocity was about 30 mm/s. Schulte-Pelkum et al. (2007(@) reported that seals can accurately track hydrodynamic trails created by another seal irrespective of their starting orientations, and even after a delay of 15-20 s. Wieskotten et al. (2010) proposed that seals use both the structure and spatial arrangement of the vortices in hydrodynamic trails for detection. Spedding (2014) provides basic scaling arguments for how the seals may be able to track a wake of a certain width. Wieskotten et al. (2011) showed that seals

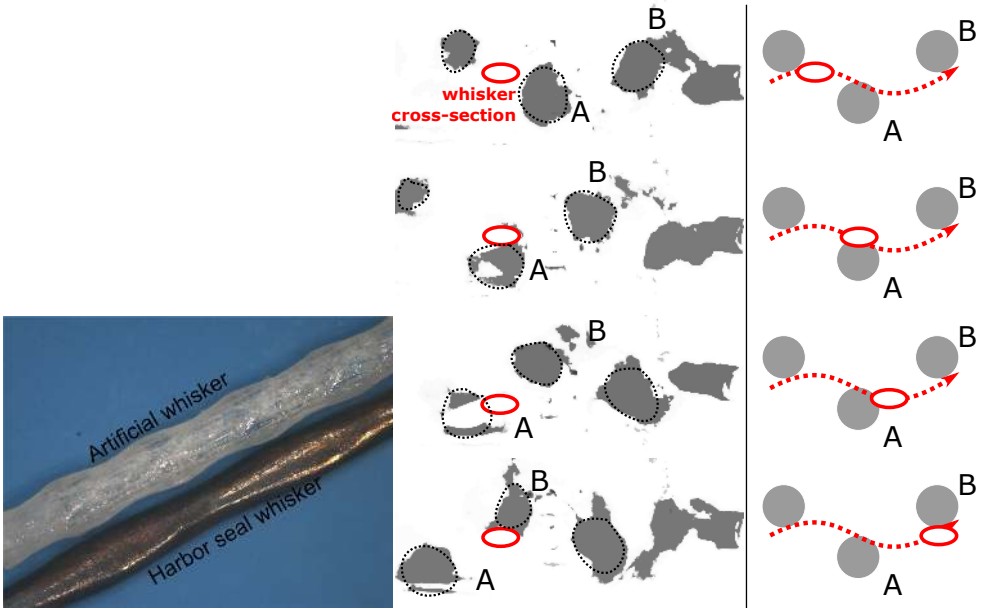

Figure 11: (Left) Sensor reproducing the harbor seal whisker shape, compared with a whisker from a harbor seal (maximum width 1.15 *mm*). (Center) Sequence of snapshots of a whisker vibrating inside the wake of an upstream cylinder; steady flow from left to right. Red ellipse depicts instantaneous position of the cross section of the whisker at the same plane as the flow visualization of oncoming vortices using upstream released dye; vortices move from left to right, shown as outlined patches. (Right) Same image as middle, keeping the vortices stationary to show the 'slaloming' path of the whisker, driving its high sensitivity of response and frequency locking (Beem & Triantafyllou 2015).

can distinguish certain towed shapes (triangle, square, etc.) based on the wake they leave.

Miersch et al. (2011) found a reduced sensitivity for sea lions compared with that of harbor seals, attributing the difference to the special, undulatory whisker shape of the latter. This unique geometry, detailed in Hanke et al. (2010), Ginter, Fish & Marshall (2010) and Ginter et al. (2012), consists of a spanwise undulatory shape with a span-varying elliptical cross-section (Figure 11). Hanke et al. (2010) showed that these undulations disrupted the coherence of the shed vortex streets and minimized the induced lift forces behind stationary whiskers. Beem & Triantafyllou (2015) conducted forced and free vibration tests on scaled up models of the harbor seals whiskers. Hans et al. (2013) conducted 3D simulations confirming the that whiskers have significantly reduced amplitude of vortex-induced vibrations (VIV), to one-tenth of that experienced by a circular cylinder. The VIV reduction occurs when the whiskers are aligned to the flow along their long axis, while when exposed at an angle of attack, significant vibrations occur.

As shown in Beem & Triantafyllou (2015), the strong directional sensitivity of the harbor seal whisker explains its ability to sense minute flows. When towed along its streamlined axis, it vibrates with amplitudes below 5% of its diameter, whereas when placed within a wake, it is also subject to a transverse flow velocity component. This causes the vibratory response to increase by an odred of magnitude; equally important is the locking-in of the

Figure 12: MEMS sensors emulating advanced biomimetic features. (Left) Hair cell-inspired NEMS sensor; a schematic showing 6 rows of PDMS polymer pillars of graded height (maximum height 425 microns). The links connecting the distal tips of the pillars are formed by polyvinylidene fluoride polymer that generates electric charges as the pillars bend causing stretching in the fibers, amplifying the signal. (Center) Photo of the implemented NEMS sensor. (right) Stereolithography fabricated whisker-like sensor on a piezoelectric diaphragm (whisker height 3 mm) (Kottapalli et al. 2014b).

frequency of whisker response to the dominant frequency of the wake. The energy extraction mechanism driving these wake-induced oscillations of a whisker when placed within an oncoming Kármán wake is a "slaloming" motion which has similarities with the motion of an energy extracting foil (Streitlien, Triantafyllou & Triantafyllou 1996; Beal et al. 2006) and a trout swimmming in the wake of a cylinder (Liao et al. 2003).

Engineering applications have emerged: Solomon & Hartmann (2006) used steel whiskers fitted with strain gauges; Stocking et al. (2010) and Eberhardt et al. (2011) proposed whisker-like sensors that used capacitance changes in a cone in cone base to measure fluid motion. Valdivia, Subramaniam & Triantafyllou (2012) developed flow sensors based specifically on the harbor seals undulatory shape. Valdivia & Bhat (2014) studied the effects of the follicle material properties on their sensitivity and range (Valdivia, Subramaniam & Triantafyllou 2013) and developed a tunable whisker sensor.

3.5. Assessment of bioinspired flow sensors

Emulating the sensing cabilities of fish will be unquestionably of great value for flow control, navigation and maneuvering of engineered vehicles and structures, and experimental fluid mechanics. However, the complexity of the structure and function of the animal organ and the processing of its information by the central nervous sytems are still not well known and understood. It will take a coordinated effort in animal studies and developing densors using novel technologies to generate a sensing capability to provide in real time a three-dimensional map of the near-field underwater environment.

For sensors mounted on the surface of a moving body, pressure sensors have an advantage over velocity sensors, as the boundary layer poses no problems for the former, as long as it remains attached, because pressure remains constant throughout the thickness of the boundary layer. Pressure sensors using a thin diaphragm have been successfully tested (Figure 10), but they suffer from the need to equilibrate the ambient pressure, particularly for deep water applications, where hydrostatic pressure is the dominant component. Biomimetically designed canal neuromast-like pressure sensors provide a fine alternative solution.

Velocity sensors similar to surface neuromasts (SN) are influenced by the boundary layer significantly; such effects vary with Reynolds number and hence with the relative speed of the body and the surrounding flow, requiring adjustment of their calibration. In addition, the sensors have to be very small, otherwise they will create a Kármán street of their own, creating significant noise in the measurements.

To emulate the sensing abilities of fish, the artificial sensors must also match the sensitivity of the lateral line, while preventing self-generating flow noise. The use of a biomimetically designed cupula-like structure, as shown in Figure 10, increased sensitivity significantly. Inspired by the fact that each haircell consists of bundles of kinocilia, which move in near unison, hence allowing the magnification of the produced signal (Corey et al. 2004), Asadnia et al. (2013c) developed a sensor consisting of graded rows of bundled polydimethylsiloxane (PDMS) polymer pillars connected at their top with polyvinylidene fluoride polymer fiber links. The links stretch and generate electric charges when the pillars, which are graded in height, bend in response to flow (Figure 12), hence amplifying the total signal significantly.

Inspired by the properties of pinniped whiskers, Kottapalli et al. (2014b) developed a neuromast microfabricated by stereolithography with an undulating shape, and placed it on a self-powered piezoelectric diaphragm sensor (Figure 12, right). The sensor demonstrated high signal to noise ratio and high directional flow-sensing capability. In addition, this sensor can be scaled up in size to measure much higher velocities, thanks to the Kármán street-canceling properties of its undulatory shape.

The study of the animal sensors reveals that the complexity of form and structure of their organs plays an important role in their outstanding sensitivity and function. Also, as more information is becoming available on how the multiple-sensor input is transmitted and processed by the central nervous system, it is anticipated that significant progress will be made in the near future towards the goal of generating a distributed touch-at-a-distance flow sensing system.

LITERATURE CITED

Abdel-Latif H, Hassan E, von Campenhausen C. 1990. Sensory performance of blind mexican cave fish after destruction of the canal neuromasts. *Naturwissenschaften* 77:237–239

Akanyeti O, Venturelli R, Visentin F, Chambers L, Megill WM, Fiorini P. 2011. What information do karman streets offer to flow sensing? *Bioinspiration & biomimetics* 6:036001

Asadnia M, Kottapalli A, Shen Z, Miao J, Barbastathis G, Triantafyllou M. 2013a. In *Micro Electro Mechanical Systems (MEMS), 2013 IEEE 26th International Conference on*. IEEE

Asadnia M, Kottapalli AGP, Shen Z, Miao J, Triantafyllou M. 2013b. Flexible and surface-mountable piezoelectric sensor arrays for underwater sensing in marine vehicles. *Sensors Journal, IEEE* 13:3918–3925

Asadnia M, Kottapalli AGP, Shen Z, Miao J, Triantafyllou M. 2013c. Flexible and surface-mountable piezoelectric sensor arrays for underwater sensing in marine vehicles. *Sensors Journal, IEEE* 13:3918–3925

Beal D, Hover F, Triantafyllou M, Liao J, Lauder G. 2006. Passive propulsion in vortex wakes. *Journal of Fluid Mechanics* 549:385–402

Beem HR, Triantafyllou MS. 2015. Exquisitely sensitive seal whisker-like sensors detect wakes at large distances. *arXiv preprint arXiv:1501.04582*

Bleckmann H, Joachim M, Coombs SL. 2014. Flow sensing in air and water

Bleckmann H, Zelick R. 1993. The responses of peripheral and central mechanosensory lateral line units of weakly electric fish to moving objects. *Journal of Comparative Physiology A* 172:115–128

Borazjani I, Sotiropoulos F, Tytell ED, Lauder GV. 2012. Hydrodynamics of the bluegill sunfish

c-start escape response: three-dimensional simulations and comparison with experimental data. *The Journal of experimental biology* 215:671–684

Bouffanais R, Weymouth GD, Yue DKP. 2010. Hydrodynamic object recognition using pressure sensing. *Proc R Soc A* 467:19–38

Chadwell BA, Standen EM, Lauder GV, Ashley-Ross MA. 2012. Median fin function during the escape response of bluegill sunfish (lepomis macrochirus). i: Fin-ray orientation and movement. *The Journal of experimental biology* 215:2869–2880

Chagnaud BP, Bleckmann H, Engelmann J. 2006. Neural responses of goldfish lateral line afferents to vortex motions. *Journal of Experimental Biology* 209:327–342

Chagnaud BP, Coombs S. 2014. In *The Lateral Line System*. Springer, 151–194

Chambers L, Akanyeti O, Venturelli R, Ježov J, Brown J, et al. 2014. A fish perspective: detecting flow features while moving using an artificial lateral line in steady and unsteady flow. *Journal of The Royal Society Interface* 11:20140467

Chen N, Tucker C, Engel JM, Yang Y, Pandya S, Liu C. 2007. Design and characterization of artificial haircell sensor for flow sensing with ultrahigh velocity and angular sensitivity. *Microelectromechanical Systems, Journal of* 16:999–1014

Conte J, Modarres-Sadeghi Y, Watts M, Hover F, Triantafyllou M. 2010. A fast-starting mechanical fish that accelerates at 40 ms- 2. *Bioinspiration & biomimetics* 5:035004

Coombs S, Bleckmann H, Fay RR, Popper AN. 2014. The lateral line system. Springer

Coombs S, Conley RA. 1997. Dipole source localization by mottled sculpin. i. approach strategies. *Journal of Comparative Physiology A: Sensory, Neural, and Behavioral Physiology* 180:387–399

Corey DP, García-Añoveros J, Holt JR, Kwan KY, Lin SY, et al. 2004. TRPA1 is a candidate for the mechanosensitive transduction channel of vertebrate hair cells. *Nature* 432:723–730

Curcic-Blake B. 2006. Source location encoding in the fish lateral line canal. *Journal of Experimental Biology* 209:1548–1559

Dagamseh A, Wiegerink R, Lammerink T, Krijnen G. 2013. Imaging dipole flow sources using an artificial lateral-line system made of biomimetic hair flow sensors. *Journal of The Royal Society Interface* 10:20130162–20130162

Dagamseh AMK, Wiegerink RJ, Lammerink TSJ, Krijnen GJM. 2012. Towards a high-resolution flow camera using artificial hair sensor arrays for flow pattern observations. *Bioinspir. Biomim.* 7:046009

Dehnhardt G. 2001. Hydrodynamic trail-following in harbor seals (phoca vitulina). *Science* 293:102–104

Dehnhardt G, Mauck B, Bleckmann H. 1998. Seal whiskers detect water movements. *Nature* 394:235–236

Domenici P. 2011. Webb scales fast-start maneuvers. *Journal of Experimental Biology* 214:875–877

Domenici P, Blake R. 1997. The kinematics and performance of fish fast-start swimming. *Journal of Experimental Biology* 200:1165–1178

Dusek J, Kottapalli AGP, Woo ME, Asadnia M, Miao J, et al. 2013. Development and testing of bio-inspired microelectromechanical pressure sensor arrays for increased situational awareness for marine vehicles. *Smart Mater. Struct.* 22:014002

Eberhardt W, Shakhsheer Y, Calhoun B, Paulus J, Appleby M. 2011. In *2011 IEEE SENSORS Proceedings*. Institute of Electrical & Electronics Engineers (IEEE)

Epps BP, Techet AH. 2007. Impulse generated during unsteady maneuvering of swimming fish. *Experiments in Fluids* 43:691–700

Fernandez VI, Maertens A, Hou S, Srivatsa K, Lang JH, Triantafyllou MS. 2011a. In *11th Intern. Conf. Fast Sea Transportation*

Fernandez VI, Maertens A, Yaul FM, Dahl J, Lang JH, Triantafyllou MS. 2011b. Lateral-line-inspired sensor arrays for navigation and object identification. *Marine Technology Society Journal* 45:130–146

Gao A, Triantafyllou M. 2012. In *2012 Oceans*. Institute of Electrical & Electronics Engineers

(IEEE)
Gazzola M, Van Rees W, Koumoutsakos P. 2012. C-start: optimal start of larval fish. *Journal of Fluid Mechanics* 698:5–18
Ginter CC, DeWitt TJ, Fish FE, Marshall CD. 2012. Fused traditional and geometric morphometrics demonstrate pinniped whisker diversity. *PLoS ONE* 7:e34481
Ginter CC, Fish FE, Marshall CD. 2010. Morphological analysis of the bumpy profile of phocid vibrissae. *Marine Mammal Science*
Hanke W, Witte M, Miersch L, Brede M, Oeffner J, et al. 2010. Harbor seal vibrissa morphology suppresses vortex-induced vibrations. *Journal of Experimental Biology* 213:2665–2672
Hans H, Miao J, Weymouth G, Triantafyllou M. 2013. In *2013 MTS/IEEE OCEANS - Bergen*. Institute of Electrical & Electronics Engineers (IEEE)
Harper DG, Blake RW. 1991. Prey capture and the fast-start performance of northern pike esox lucius. *Journal of experimental Biology* 155:175–192
Hassan ES. 1993. Mathematical description of the stimuli to the lateral line system of fish, derived from a three-dimensional flow field analysis. III. the case of an oscillating sphere near the fish. *Biol. Cybern.* 69:525–538
Huffard CL. 2006. Locomotion by abdopus aculeatus (cephalopoda: Octopodidae): walking the line between primary and secondary defenses. *J. Expl. Biol.* 209:3697–3707
Klein A, Bleckmann H. 2011. Determination of object position, vortex shedding frequency and flow velocity using artificial lateral line canals. *Beilstein Journal of Nanotechnology* 2:276–283
Kottapalli AGP, Tan CW, Olfatnia M, Miao JM, Barbastathis G, Triantafyllou M. 2011. A liquid crystal polymer membrane MEMS sensor for flow rate and flow direction sensing applications. *Journal of Micromechanics and Microengineering* 21:085006
Kottapalli AGP, Asadnia M, Miao JM, Barbastathis G, Triantafyllou MS. 2012a. A flexible liquid crystal polymer MEMS pressure sensor array for fish-like underwater sensing. *Smart Mater. Struct.* 21:115030
Kottapalli A, Asadnia M, Barbastathis G, Triantafyllou M, Miao J, Tan C. 2012b. Polymer MEMS pressure sensor arrays for fish-like underwater sensing applications. *Micro & Nano Letters* 7:1189–1192
Kottapalli AGP, Asadnia M, Miao JM, Triantafyllou MS. 2013. In *2013 IEEE 26th International Conference on Micro Electro Mechanical Systems (MEMS)*. Institute of Electrical & Electronics Engineers (IEEE)
Kottapalli AGP, Asadnia M, Miao J, Triantafyllou M. 2014a. Touch at a Distance Sensing: Lateral-Line inspired MEMS Flow Sensors. *Bioinsp. and Biom.* 9:046011
Kottapalli AGP, Asadnia M, Hans H, Miao J, Triantafyllou M. 2014b. In *2014 IEEE 27th International Conference on Micro Electro Mechanical Systems (MEMS)*. Institute of Electrical & Electronics Engineers (IEEE)
Kriegseis J, Kinzel M, Rival DE. 2013. On the persistence of memory: do initial conditions impact vortex formation? *Journal of Fluid Mechanics* 736:91–106
Liao JC. 2006. The role of the lateral line and vision on body kinematics and hydrodynamic preference of rainbow trout in turbulent flow. *Journal of Experimental Biology* 209:4077–4090
Liao JC. 2007. A review of fish swimming mechanics and behaviour in altered flows. *Philosophical Transactions of the Royal Society B: Biological Sciences* 362:1973–1993
Liao JC, Beal DN, Lauder GV, Triantafyllou M. 2003. Fish exploiting vortices decrease muscle activity. *Science* 302:1566–1569
Liu C. 2007. Micromachined biomimetic artificial haircell sensors. *Bioinspir. Biomim.* 2:S162–S169
Maertens AP, Triantafyllou MS. 2014. The boundary layer instability of a gliding fish helps rather than prevents object identification. *Journal of Fluid Mechanics* 757:179–207
McConney ME, Anderson KD, Brott LL, Naik RR, Tsukruk VV. 2009a. Bioinspired material approaches to sensing. *Advanced Functional Materials* 19:2527–2544
McConney ME, Chen N, Lu D, Hu HA, Coombs S, et al. 2009b. Biologically inspired design of

hydrogel-capped hair sensors for enhanced underwater flow detection. *Soft Matter* 5:292
McHenry MJ, Liao JC. 2014. In *The Lateral Line System*. Springer, 73–98
Miao J, Kottapalli AGP, Asadnia M, Triantafyllou MS. 2013. *SPIE Newsroom*, (doi:10.1117/2.1201302.004734).
Miersch L, Hanke W, Wieskotten S, Hanke FD, Oeffner J, et al. 2011. Flow sensing by pinniped whiskers. *Philosophical Transactions of the Royal Society B: Biological Sciences* 366:3077–3084
Mogdans J, Bleckmann H. 1998. Responses of the goldfish trunk lateral line to moving objects. *Journal of Comparative Physiology A: Sensory, Neural, and Behavioral Physiology* 182:659–676
Montgomery J, Coombs S, Halstead M. 1995. Biology of the mechanosensory lateral line in fishes. *Rev Fish Biol Fisheries* 5:399–416
Montgomery JC, Baker CF, Carton AG. 1997. The lateral-line can mediate rheotaxis in fish. *Nature* 389:960–963
Montgomery JC, Coombs S, Baker CF. 2001. In *The biology of hypogean fishes*. Springer Science & Business Media, 87–96
Müller H, Fleck A, Bleckmann H. 1996. The responses of central octavolateralis cells to moving sources. *Journal of Comparative Physiology A* 179
Müller UK, van den Boogaart JGM, van Leeuwen JL. 2008. Flow patterns of larval fish: undulatory swimming in the intermediate flow regime. *Journal of Experimental Biology* 211:196–205
Niesterok B, Hanke W. 2012. Hydrodynamic patterns from fast-starts in teleost fish and their possible relevance to predator–prey interactions. *Journal of Comparative Physiology A* 199:139–149
Packard A. 1969. Jet propulsion and the giant fibre response of loligo. *Nature* 221:875–877
Pitcher T, Partridge B, Wardle C. 1976. A blind fish can school. *Science* 194:963–965
Plachta DTT. 2003. A hydrodynamic topographic map in the midbrain of goldfish carassius auratus. *Journal of Experimental Biology* 206:3479–3486
Rapo MA, Jiang H, Grosenbaugh MA, Coombs S. 2009. Using computational fluid dynamics to calculate the stimulus to the lateral line of a fish in still water. *Journal of Experimental Biology* 212:1494–1505
Ren Z, Mohseni K. 2012. A model of the lateral line of fish for vortex sensing. *Bioinspir. Biomim.* 7:036016
Ristroph L, Liao JC, Zhang J. 2015. Lateral line layout correlates with the differential hydrodynamic pressure on swimming fish. *Phys. Rev. Lett.* 114
Salumae T, Kruusmaa M. 2013. Flow-relative control of an underwater robot. *Proceedings of the Royal Society A: Mathematical, Physical and Engineering Sciences* 469:20120671–20120671
Schulte-Pelkum N, Wieskotten S, Hanke W, Dehnhardt G, and Mauck B. 2007. Tracking of biogenic hydrodynamic trails in harbour seals (phoca vitulina). *J Exp Biol* 210:781–787
Sichert A, Bamler R, van Hemmen J. 2009. Hydrodynamic object recognition: When multipoles count. *Phys. Rev. Lett.* 102
Solomon JH, Hartmann MJ. 2006. Biomechanics: Robotic whiskers used to sense features. *Nature* 443:525–525
Spagnolie SE, Shelley MJ. 2009. Shape-changing bodies in fluid: hovering, ratcheting, and bursting. *Physics of Fluids (1994-present)* 21:013103
Spedding GR. 2014. Wake signature detection. *Annu. Rev. Fluid Mech.* 46:273–302
Stocking JB, Eberhardt WC, Shakhsheer YA, Calhoun BH, Paulus JR, Appleby M. 2010. In *2010 IEEE Sensors*. Institute of Electrical & Electronics Engineers (IEEE)
Streitlien K, Triantafyllou GS, Triantafyllou MS. 1996. Efficient foil propulsion through vortex control. *AIAA Journal* 34:2315–2319
Tao J, Yu XB. 2012. Hair flow sensors: from bio-inspiration to bio-mimicking—a review. *Smart Mater. Struct.* 21:113001
Taylor G. 1953. Formation of a vortex ring by giving an impulse to a circular disk and then dissolving it away. *Journal of Applied Physics* 24:104–104

Triantafyllou MS. 2012. Survival hydrodynamics. *Journal of Fluid Mechanics* 698:1–4

Tytell ED, Lauder GV. 2008. Hydrodynamics of the escape response in bluegill sunfish, lepomis macrochirus. *Journal of Experimental Biology* 211:3359–3369

Valdivia P, Bhat S. 2014. In *Bioinspiration, Biomimetics, and Bioreplication 2014*, ed. A Lakhtakia. SPIE-Intl Soc Optical Eng

Valdivia P, Subramaniam V, Triantafyllou M. 2012. In *2012 IEEE Sensors*. Institute of Electrical & Electronics Engineers (IEEE)

Valdivia P, Subramaniam V, Triantafyllou M. 2013. In *2013 IEEE/RSJ International Conference on Intelligent Robots and Systems*. Institute of Electrical & Electronics Engineers (IEEE)

van Netten SM. 2006. Hydrodynamic detection by cupulae in a lateral line canal: functional relations between physics and physiology. *Biol Cybern* 94:67–85

Venturelli R, Akanyeti O, Visentin F, Ježov J, Chambers LD, et al. 2012. Hydrodynamic pressure sensing with an artificial lateral line in steady and unsteady flows. *Bioinspir. Biomim.* 7:036004

Von Campenhausen C, Riess I, Weissert R. 1981. Detection of stationary objects by the blind cave fishanoptichthys jordani (characidae). *Journal of comparative physiology* 143:369–374

Wakeling JM, Johnston I. 1998. Muscle power output limits fast-start performance in fish. *Journal of Experimental Biology* 201:1505–1526

Webb JF. 2014a. In *Flow Sensing in Air and Water*. Springer Science & Business Media, 247–270

Webb JF. 2014b. In *The Lateral Line System*. Springer Science & Business Media, 17–72

Webb P. 1976. The effect of size on the fast-start performance of rainbow trout salmo cairdneri, and a consideration of piscivorous predator-prey interactions. *Journal of Experimental Biology* 65:157–177

Weihs D. 1973. The mechanism of rapid starting of slender fish. *Biorheology* 10:343–350

Weihs D, Webb PW. 1984. Optimal avoidance and evasion tactics in predator-prey interactions. *Journal of Theoretical Biology* 106:189–206

Wells M. 1990. Oxygen extraction and jet propulsion in cephalopods. *Canadian Journal of Zoology* 68:815–824

Weymouth GD, Subramaniam V, Triantafyllou MS. 2015. Ultra-fast escape maneuver of an octopus-inspired robot. *Bioinspir. Biomim.* 10:016016

Weymouth GD, Triantafyllou MS. 2012. Global vorticity shedding for a shrinking cylinder. *Journal of Fluid Mechanics* 702:470–487

Weymouth GD, Triantafyllou MS. 2013. Ultra-fast escape of a deformable jet-propelled body. *Journal of Fluid Mechanics* 721:367–385

Wieskotten S, Dehnhardt G, Mauck B, Miersch L, Hanke W. 2010. Hydrodynamic determination of the moving direction of an artificial fin by a harbour seal (phoca vitulina). *J Exp Biol* 213:2194–2200

Wieskotten S, Mauck B, Miersch L, Dehnhardt G, Hanke W. 2011. Hydrodynamic discrimination of wakes caused by objects of different size or shape in a harbour seal (phoca vitulina). *Journal of Experimental Biology* 214:1922–1930

Windsor SP, Norris SE, Cameron SM, Mallinson GD, Montgomery JC. 2010. The flow fields involved in hydrodynamic imaging by blind mexican cave fish (astyanax fasciatus). part II: gliding parallel to a wall. *Journal of Experimental Biology* 213:3832–3842

Wu G, Yang Y, Zeng L. 2007. Routine turning maneuvers of koi carp cyprinus carpio koi: effects of turning rate on kinematics and hydrodynamics. *Journal of Experimental Biology* 210:4379–4389

Yang Y, Chen J, Engel J, Pandya S, Chen N, et al. 2006. Distant touch hydrodynamic imaging with an artificial lateral line. *Proceedings of the National Academy of Sciences* 103:18891–18895

Yang Y, Klein A, Bleckmann H, Liu C. 2011. Artificial lateral line canal for hydrodynamic detection. *Applied Physics Letters* 99:023701

Zhu Q, Wolfgang M, Yue DKP, Triantafyllou MS. 2002. Three-dimensional flow structures and vorticity control in fish-like swimming. *Journal of Fluid Mechanics* 468:1–28